Electron tunneling in respiratory complex I

Tomoyuki Hayashi and Alexei A. Stuchebrukhov[1]

Department of Chemistry, University of California, Davis, CA 95616

Edited by Harry B. Gray, California Institute of Technology, Pasadena, CA, and approved September 14, 2010 (received for review June 25, 2010)

NADH:ubiquinone oxidoreductase (complex I) plays a central role in the respiratory electron transport chain by coupling the transfer of electrons from NADH to ubiquinone to the creation of the proton gradient across the membrane necessary for ATP synthesis. Here the atomistic details of electronic wiring of all Fe/S clusters in complex I are revealed by using the tunneling current theory and computer simulations; both density functional theory and semiempirical electronic structure methods were used to examine antiferromagnetically coupled spin states and corresponding tunneling wave functions. Distinct electron tunneling pathways between neighboring Fe/S clusters are identified; the pathways primarily consist of two cysteine ligands and one additional key residue. Internal water between protein subunits is identified as an essential mediator enhancing the overall electron transfer rate by almost three orders of magnitude to achieve a physiologically significant value. The identified key residues are further characterized by sensitivity of electron transfer rates to their mutations, examined in simulations, and their conservation among complex I homologues. The unusual electronic structure properties of Fe_4S_4 clusters in complex I explain their remarkable efficiency of electron transfer.

electron transfer in proteins | respiratory chain | iron-sulfur clusters

NADH:ubiquinone oxidoreductase (complex I) is a large L-shaped membrane-bound enzyme involved in cellular respiration that catalyzes the oxidation of NADH and the reduction of ubiquinone in mitochondria and respiring bacteria (1–3). This reaction involves the transfer of electrons over approximately 90 Å from NADH bound to the hydrophilic domain to ubiquinone in or near the hydrophobic membrane-bound domain of complex I (4). In turn, the reaction provides the driving force for translocation of four protons across the membrane, thus generating, in part, the proton gradient necessary for ATP synthesis (5). Complex I defects are the cause of several neurodegenerative diseases including Parkinson disease, Alzheimer's disease, and Huntington disease (6).

The transfer of electrons from NADH to ubiquinone is facilitated by flavin mononucleotide (FMN), two binuclear (2Fe-2S) iron-sulfur clusters (N1a and N1b), and six tetranuclear (4Fe-4S) iron-sulfur clusters (N3, N4, N5, N6a, N6b, and N2) (Fig. 1*A*). NADH, a two-electron donor, initially passes both electrons, as hydride, to the FMN cofactor. From FMN one electron enters a transport chain leading to the ubiquinone-binding site; the second electron enters a side path to N1a that appears to serve as a control mechanism to prevent generation of superoxide ions (4).

The crystal structure of hydrophilic domain of complex I from *Thermus thermophilus* was reported in 2006 (4), and recently the whole architecture of the enzyme has been revealed (7); however, until now, the atomistic details of electron transfer along the chain of Fe/S metal clusters have remained unknown. Recently, a hopping (stepwise) electron transfer (ET) mechanism involving aromatic amino acids has been proposed (8) to explain the high overall transport rate (estimated as ~170 s^{-1} in refs. 9 and 10 and ~10^4 s^{-1} in ref. 11). However, in that study, the internal water has not been taken into account, whereas it is known that water in proteins is capable of accelerating electron transfer (12–15). In this paper we use state-of-the-art electronic structure calculations to show that the mechanism of electron transfer is quantum mechanical tunneling, as in the rest of electron transport chain; the water between subunits of complex I plays the critical role in mediating electron transport.

Fe/S clusters have unique electronic properties due to the antiferromagnetically coupled high-spin iron atoms (16–19). The main feature of such clusters is the exceptionally high quasi degeneracy of the electronic states, which has its origin in the fivefold degeneracy of the *d*-orbitals of Fe ions. As a consequence, many quasi-degenerate electronic states are present within the energy interval of a few k_BT above the ground state and hence are dynamically accessible. The qualitative energy level diagram of the reduced $[Fe_4S_4(SH_3)_4]^{3-}$ model cluster shows that the electronic spin states in fact form a dense quasi continuum (Fig. 1*B*). According to the Marcus electron transfer theory (20), such an unusual electronic structure should have a direct consequence for the efficiency of electron transfer.

Here we use both density functional theory (DFT) and a semiempirical electronic structure method, Zerner's intermediate neglect of differential overlap (ZINDO), to examine the tunneling pathways and the strength of electronic coupling between Fe/S clusters in complex I. The method is based on the analysis of so-called broken-symmetry (BS) states (17) of the donor and acceptor quasi-continuum "bands" to obtain a dynamically averaged picture.

ZINDO has been successfully applied to simulate the spin states and the electronic spectra of transition metal complexes with an accuracy comparable to that of DFT (time-dependent DFT for spectra) (21–23). The Heisenberg spin Hamiltonian and the resulting spin states of polynuclear transition metal complexes computed with ZINDO agree well with the experimental data (24). ZINDO also reproduces the electronic absorption spectra of mononuclear and binuclear Fe/S clusters (25). ZINDO has also been extensively used for calculations of electron transfer in a variety of inorganic and organic systems (26); the method has an advantage in describing the through-space interactions of noncovalently bonded protein atoms because of its Slater-type orbitals (27). The calculated BS ground state of isolated $[Fe_4S_4(SCH_3)_4]^{3-}$ at the ZINDO level with an optimized geometry by BS-DFT calculation (28) captures the antiferromagnetic spin structure with two iron sites spin up and two iron sites spin down in agreement with the BS-DFT calculations of ref. 17. The calculated BS highest occupied molecular orbital (HOMO), which contributes most to the electron tunneling, is a combination of Fe-Fe σ^* and S-S σ^*, in agreement with one of the two spin states coexisting at room temperature (17). Fig. 1 *C1* and *C2* shows that both DFT and ZINDO produce similar results, suggesting the reasonable accuracy of ZINDO, comparable to that of DFT.

The simulations of electron transfer between redox centers are based on the tunneling current theory (29, 30), which had been successfully applied to several systems previously. The theory

Author contributions: T.H. and A.A.S. designed research; T.H. performed research; T.H. contributed new reagents/analytic tools; T.H. and A.A.S. analyzed data; and T.H. and A.A.S. wrote the paper.

The authors declare no conflict of interest.

This article is a PNAS Direct Submission.

[1]To whom correspondence should be addressed. E-mail: stuchebr@chem.ucdavis.edu.

This article contains supporting information online at www.pnas.org/lookup/suppl/doi:10.1073/pnas.1009181107/-/DCSupplemental.

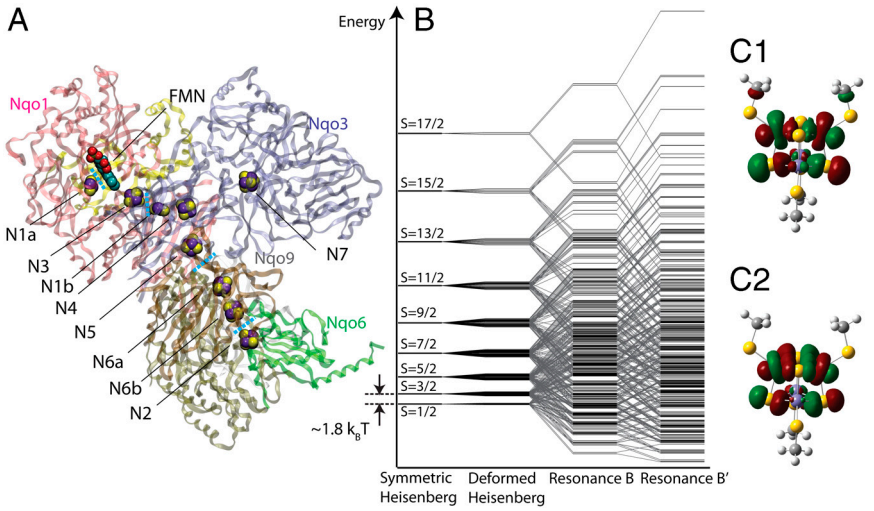

Fig. 1. (*A*) Crystal structure of the hydrophilic domain of the respiratory complex I from *T. thermophilus* (4). Cluster N1a is in subunit Nqo2, N3 and FMN in Nqo1, N1b, N4, N5, and N7 in Nqo3, N6a/b in Nqo9, and N2 in Nqo6. (*B*) Spin state diagram of the $[Fe_4S_4(SCH_3)_4]^{3-}$ cluster. (See *SI Text* for details.) The total 3,000 states are grouped by total spin *S* to 380 clusters overlapping in energy (17). The experimental value of the Heisenberg constant *J* is 250 cm^{-1}; a few tens of low-lying states contribute to the electron tunneling. (*C1* and *C2*) HOMO of the $[Fe_4S_4(SCH_3)_4]^{3-}$ BS ground electronic states calculated with DFT (B3LYP) and ZINDO, respectively.

treats many-electron wave functions explicitly by incorporating both the tunneling electron orbitals and the induced polarization of core electrons. By assuming single Slater determinant many-electron wave functions of the donor and acceptor diabatic states, the donor and acceptor tunneling orbitals that carry the tunneling electron are obtained as biorthogonal donor and acceptor orbitals with the smallest overlap (29, 31). The rest of the orbitals undergoing induced polarization in the tunneling transition give rise to the electronic Franck–Condon factor (30, 31). The calculations focus on the evaluation of the transition flux between donor $|D\rangle$ and acceptor $|A\rangle$ electronic states:

$$\vec{J}(r) = -i\langle A|\hat{\vec{j}}(r)|D\rangle, \quad [1]$$

where $\hat{j}$ is the quantum flux operator. The coarse graining of the flux results in so-called interatomic currents J_{ab}, which describe the tunneling flux at the atomic level (30). The total current through a given atom is proportional to the probability that the tunneling electron passes through it in the tunneling jump from donor to acceptor (Fig. 2). Tunneling matrix element T_{DA} is calculated by using the tunneling flux theorem as the total flux across the dividing plane between the donor and acceptor (see Fig. S1) (29, 30):

$$T_{DA} = -\hbar \int (d\vec{s}\cdot\vec{J}). \quad [2]$$

To simplify computationally intensive all-electron calculations, a protein-pruning procedure was performed for each pair of neighboring Fe/S clusters as described in ref. 32. The resulting pruned systems contain 200–500 atoms. Subsequent BS-ZINDO calculations give low-lying 1–3 BS states for each Fe/S cluster. Tunneling calculations are performed for possible pairs of donor and acceptor BS states.

Results and Discussion

Electron Tunneling Pathways. For different pairs of donor and acceptor BS states, the tunneling pathways are mainly similar, except for some details at the Fe/S clusters themselves. Most typical tunneling pathways are shown in Fig. 2.

FMN and N3 are both located in subunit Nqo1. The electron tunnels from FMN to N3 primarily through the δ-methyl group of $_1$Leu^{402} (the prefix indicates subunit number) with two short through-space jumps of 2.9 and 2.4 Å. There is a secondary pathway through the γ-carbon of $_1$Glu^{184} with longer through-space jumps of 2.9 and 3.2 Å. The preference of the pathways is justified by the total distance of the tunneling trajectory from edge to edge: The primary path of 7.5 Å is much shorter than the secondary path of 13.3 Å.

Clusters N3 and N1b, located in subunit Nqo1 and Nqo3, respectively, have a center-to-center distance of 14.0 Å. Two cysteine ligands ($_1$Cys^{356} and $_1$Cys^{359}) of N3 are connected by neighboring $_1$Thr^{357} and $_1$Pro^{358} to make a backbone loop (N3-$_1$Cys^{356}-$_1$Thr^{357}-$_1$Pro^{358}-$_1$Cys^{359}-N3), with $_1$Cys^{356}, $_1$Thr^{357}, and $_1$Pro^{358} exposed to the subunit boundary of Nqo1 and Nqo3. N1b complex has $_3$Cys^{64} cysteine ligand oriented toward N3, of which the amide C=O group together with neighboring $_3$Ala^{63} and $_3$Arg^{65} is facing the subunit boundary. The tunneling current flows from N3 along the backbone loop of $_1$Cys^{356} → $_1$Thr^{357} → $_1$Pro^{358} → $_1$Cys^{359} back to N3. A part of the loop current is transmitted from $_1$Cys^{356} and $_1$Thr^{357} to $_3$Ala^{63}-$_3$Cys$_{64}$ wire aligned in parallel across the subunit boundary. The main pathway from N3 to N1b is through $_1$Cys^{356} and $_3$Cys^{64} with a 2.8-Å through-space jump.

Clusters N1b and N4 are both located in subunit Nqo3 and have a 13.5-Å center-to-center distance. Cysteine ligands of N1b and N4 ($_3$Cys^{34} and $_3$Cys^{184}) are oriented along the connecting line of N1b and N4 and are spatially contacted. The main electron tunneling pathway of N1b → N4 is along $_3$Cys^{34} and $_3$Cys^{184} with a 1.9-Å through-space jump.

Clusters N4 and N5 are both located in Nqo3 and have a 12.2-Å center-to-center distance. $_3$Val^{232} is located in the middle of N4 and N5 with two γ-methyl groups oriented toward N4 and N5 complexes. The main tunneling pathway is through the isopropyl side chain of $_3$Val^{232} with two through-space jumps from N4 to $_3$Val^{232} (3.0 Å) and from $_3$Val^{232} to N5 (2.2 Å). When Fe2 (N4) is mainly donating the tunneling electron, there is a side path along the $_3$His^{115} ligand of N5 and the $_3$Cys^{181} ligand of N4 with a 3.0-Å through-space jump in a destructive quantum interference.

Clusters N5 and N6a, located in subunits Nqo3 and Nqo9, respectively, have the largest center-to-center distance of 16.8 Å. N5 has two cysteine ($_3$Cys^{119} and $_3$Cys^{122}) wires connected by neighboring $_3$Pro^{120} and $_3$Thr^{121} residues making the same type of backbone loop (N5-$_3$Cys^{119}-$_3$Pro^{120}-$_3$Thr^{121}-$_3$Cys^{122}-N5) as

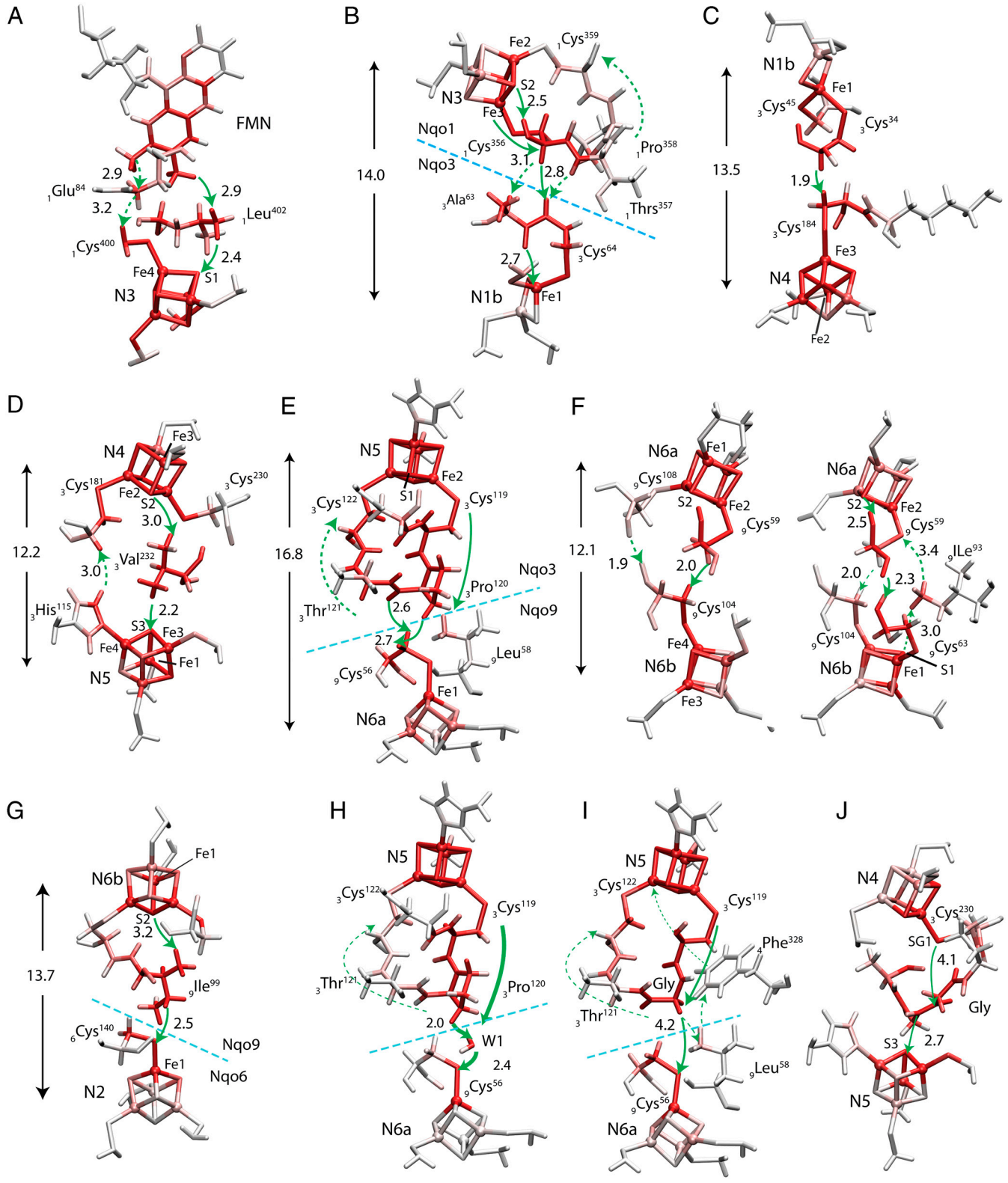

Fig. 2. Electron tunneling pathways of (*A*) FMN → N3, (*B*) N3 → N1b, (*C*) N1b → N4, (*D*) N4 → N5a, (*E*) N5 → N6a, (*F*) N6a → N6b, (*G*) N6b → N2, (*H*) N5 → N6a with structural water at the protein subunit boundary, (*I*) N5 → N6a with a $_3$Pro^{120} to Gly mutation, and (*J*) N4 → N5 with a $_3$Val^{232} to Gly mutation. Total atomic current proportional to the probability that the tunneling electron will pass through a given atom ($J_a^{tot} = \sum_b |J_{ab}|/2$) is indicated by red color intensity. Through-space jumps are indicated by green arrows with distances in angstroms. When multiple paths present, directions of the electron flux in the primary and secondary paths are marked by solid and dashed arrows, respectively. The arrows and numbers in angstroms are center-to-center distances between the donor and acceptor clusters.

with N3. The loop is stabilized by a hydrogen bond between the carbonyl oxygen of $_3$Cys^{119} and the amide N-H of $_3$Thr^{121}. The main electron tunneling flux from N5 is through $_3$Cys^{119} and $_3$Pro^{120}, part of which is reflected back to N5 through $_3$Thr^{121}

and $_3$Cys^{122}; the rest is transmitted to $_9$Cys^{56} with a 2.7- or 2.6-Å through-space jump across the subunit boundary of Nqo3 and Nqo9. The electron then tunnels through the $_9$Cys^{56} ligand to reach Fe1(N6a).

Clusters N6a and N6b located in subunit Nqo9 have the closest distance of 12.1 Å. A cysteine ligand $_9$Cys^{59} of N6a has a spatial contact with two cysteine ligands ($_9$Cys^{104} and $_9$Cys^{63}) of N6b. The $_9$Cys^{108} ligand of N6a is also in contact with the $_9$Cys^{104} ligand of N6b. In the case when Fe4(N6b) and Fe3(N6b) are mainly reduced, the primary tunneling pathway from N6a to N6b is through $_9$Cys^{59} and $_9$Cys^{104} with a 2.0-Å through-space jump with a minor flux along $_9$Cys^{108} and $_9$Cys^{104}. When mainly Fe1(N6b) accepts the electron, the primary pathway is through $_9$Cys^{59} and $_9$Cys^{63} with a 2.3-Å through-space jump with a significant tunneling flux along $_9$Ile^{93} in a destructive quantum interference.

Clusters N6b and N2, located in subunits Nqo9 and Nqo6, respectively, have a distance of 13.7 Å. In this case, the tunneling electron first makes a 3.2-Å through-space jump from S2 of N6b to γ-methyl hydrogen of $_9$Ile^{99}. The electron then follows the alkyl chain of $_9$Ile^{99} to the γ-methylene group and makes the second 3.4-Å through-space jump to the $_6$Cys^{140} ligand of N2.

The whole electronic wiring of complex I is obtained by combining tunneling pathways of individual processes, as shown in Fig. 3. It is clear that specific peptide residues serve as electronic wires connecting neighboring Fe/S clusters; individual electron tunneling paths involve up to three protein residues, including two cysteine ligands and one additional key residue (Table 1). Notably, the clusters in the protein are oriented in a specific way—corner to corner—with Cys ligands mostly pointing toward each other, which is clearly the most efficient way to transfer electrons from one cluster to another.

Electron Transfer Rates. The electron transfer rates between the clusters are calculated by using Marcus's theory (20)

$$k_{\mathrm{ET}} = \frac{2\pi}{\hbar}\frac{\langle T_{DA}{}^2\rangle}{\sqrt{4\pi\lambda k_{\mathrm{B}}T}}\exp\left[-\frac{(\Delta G^0+\lambda)^2}{4\lambda k_{\mathrm{B}}T}\right], \qquad [3]$$

with a generic reorganization energy $\lambda = 0.5$ eV (33, 34) and the driving force $\Delta G = 0$ eV for all processes with an exception of $\Delta G = -0.15$ eV for N6b → N2 (1, 35). The electronic coupling matrix elements T_{DA} were calculated as described in *SI Text*. Different nearly degenerate electronic states are typically localized differently in the Fe/S cluster because of the antiferromagnetism; this means that the tunneling orbitals in the core regions are constantly changing on the time scale of thermal dynamics of the local protein environment, which is much faster than that of the slowest electron transfer. The dynamical and statistical average of the tunneling matrix element (36) is described in terms of the renormalized value $\langle T_{DA}{}^2\rangle$.

The averaging procedure reflects the fact that many tunneling orbitals are statistically mixed in the course of protein dynamics (see Fig. S2). This averaging helps to rationalize the long-standing puzzle as to why the electron transfer rates in proteins best correlate with edge-to-edge distance between redox cofactors (33, 37); it also explains the efficiency of Fe/S clusters to pass tunneling electrons along the chain: If there were no mixing of the electronic states, the incoming and outgoing electrons would tunnel from the same gateway atom of a cluster, which obviously is very inefficient because of the additional tunneling distance.

The calculated electronic couplings and the rates are shown in Table 1. Four electron transfer processes of N1b → N4, N4 → N5, N6a → N6b, and N6b → N2 are faster than both the reported estimates of the total transfer rate: 170 and 10^4 s^{-1}. However, the transfer rate of N3 → N1b ($\sim 10^3$ s^{-1}) is slower than the highest estimate, and N5 → N6a (~ 10 s^{-1}) is drastically slower than the reported rates, which indicates that an important factor is missing in the model. The pathway analysis shows that the two slowest processes N5 → N6a and N3 → N1b are controlled by the rate of electron tunneling across protein subunit boundaries where internal water molecules should be present (14). In the reported structure, however, the intervening water is not seen, which suggests its significant mobility.

Enhancement of Electron Transfer Rates due to the Internal Water. To examine the hypothesis that the internal water at the interface between the enzyme subunits should facilitate the intersubunit electron tunneling, the following simulations were performed. For pairs N3 → N1b, N5 → N6a, and N6b → N2, which involve intersubunit transfers (Fig. 3), water molecules were placed along the tunneling pathways at the interface between the subunits; the structure was optimized by using molecular dynamics simulations. With water present between the subunits, the tunneling rates are dramatically increased by two to three orders of magnitude (Table 1). For the slowest transfer N5 → N6a, along the path ($_3$Cys^{119} → $_3$Pro^{120} → $_9$Cy^{56}) (Fig. 2*H*), the tunneling rate is accelerated to 0.73×10^4 s^{-1}. With this increase, the overall transfer rate now satisfies a typical physiological requirement (33) and is roughly equal to a typical electron transfer rate for such distance (37). With the water included, the overall negative slope of the distance dependence also becomes close to a typical 1.4 in natural logarithm (or 0.6 in base 10 logarithm) (Fig. 4); however, without water, the slope is in the range of 1.8–2.3 (Fig. S3), indicating the empty spaces in the protein structure (37). The internal water at the subunit boundaries is therefore an essential mediator for the efficient electron transfer along the redox chain of complex I. The calculated enhancement of the ET rate due to the internal water

Table 1. Distances, key residues, couplings $\langle T_{DA}{}^2\rangle$, and calculated rates k_{ET} of ET in complex I

	Distance, Å		Key residues				
Pair	C-to-C	G-to-G	Exit	Entrance	Mediator	$\langle T_{DA}{}^2\rangle$, cm^{-2}	k_{ET}, s^{-1}
N3 → N1b	14.0	11.0–12.6	$_1$Cys^{356}	$_3$Cys^{64}	$_3$Ala^{63}	$4.6 \times 10^{-4}(1.1)$	$1.3 \times 10^3(2.9 \times 10^6)$
N1b → N4	13.5	10.6	$_3$Cys^{34}	$_3$Cys^{184}	—	2.3×10^{-2}	6.4×10^4
N4 → N5	12.2	8.7	—	—	$_3$Val^{232}	9.8	2.8×10^7
N5 → N6a	16.8	14.0	$_3$Cys^{119}	$_9$Cys^{56}	$_3$Pro^{120}	$3.2 \times 10^{-6}(2.3 \times 10^{-3})$	$9.1(7.3 \times 10^3)$
N6a → N6b	12.1	9.3–11.1	$_9$Cys^{59}	$_9$Cys^{104}	—	0.98	2.8×10^6
N6b → N2	13.7	10.5	—	$_6$Cys^{140}	$_9$Ile^{99}	$5.8 \times 10^{-4}(5.3 \times 10^{-2})$	$1.9 \times 10^4(1.8 \times 10^6)$
(N4 → N5)*	12.2	8.7	—	—	Gly	8.0×10^{-3}	2.3×10^4
(N5 → N6a)*	16.8	14.0	$_3$Cys^{119}	$_9$Cys^{56}	Gly	$4.1 \times 10^{-7}(7.6 \times 10^{-5})$	$1.2(0.3 \times 10^2)$

(C-to-C) and (G-to-G) are center-to-center and gateway-to-gateway atom distances, respectively. The gateway atoms are defined as core atoms of Fe/S clusters that give the largest contribution to the transition. The key residues of the main tunneling path are defined as "exit," a ligand of the donor, "entrance," a ligand of the acceptor, if they participate, and a "mediator," if there is one. For couplings and rates, the numbers without parentheses are for the "dry" protein, and the numbers in parentheses are for the protein with structural water included. (N4 → N5)* is for N4 → N5 with a $_3$Val^{232} to glycine substitution. (N5 → N6a)* is for N5 → N6a with a $_3$Pro^{120} to glycine substitution.

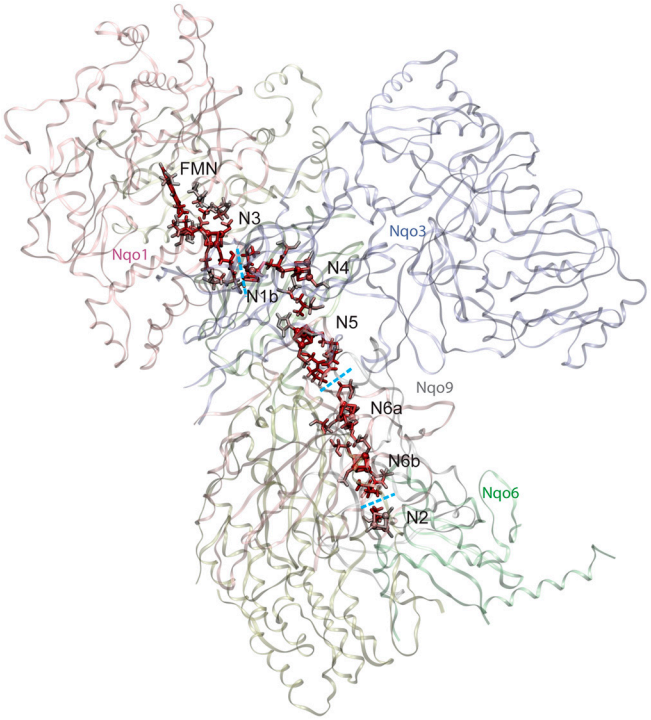

Fig. 3. Calculated complete electron tunneling pathways from FMN to N2 of complex I. The atoms with significant electron tunneling probability are highlighted with red color intensity corresponding to their total atomic currents. The dashed lines indicate the subunit boundaries.

agrees well with a recent study on the bovine liver cytochrome b_5 (12).

Mutations of Key Residues. The key residues identified in this study as mediators of electron transfer (Table 1) are remarkably conserved among different organisms. In the primary sequence among 11 complex I homologues (see Fig. S4), $_3$Pro^{120} of the main tunneling pathway connecting N5 and N6a is conserved with only one exception of *Rhodobacter sphaeroides*, where it is replaced by an alanine. $_3$Pro^{120} is an exit of the peptide backbone loop (N5-$_3$Cys^{119}-$_3$Pro^{120}-$_3$Thr^{121}-$_3$Cys^{122}-N5) where an electron is transmitted to $_9$Cys^{56} through water at the protein subunit boundary. $_3$Pro^{120} is also important to give rigidity to the backbone loop, by keeping its pyrrolidine ring near $_9$Cys^{56} in an optimal position for electron transfer. The less significant neighboring $_3$Thr^{121} is not conserved and is replaced by a valine or an isoleucine in other species. The idea is supported by the simulation of a $_3$Pro^{120} to Gly mutant; in this mutant the electron tunneling rate is decreased from 9.1 to 1.2 s^{-1} when internal water is not present and from 7,300 to 30 s^{-1} when internal water is present (Table 1). Such a dramatic decrease in the overall electron transfer rate should be detrimental to the physiological function of complex I.

The electron tunneling of N4 → N5 is unique in that a single side chain of $_3$Val^{232} mediates the tunneling path (Fig. 2*D*). The sequence analysis shows that $_3$Val^{232} is well conserved except for *Escherichia coli* and *R. sphaeroides*, where $_3$Val^{232} is replaced by a threonine. This substitution, however, is consistent with the role that this group plays in mediating electron transfer: The Y-shaped isopropyl side chain of the valine is optimal for extending two γ-methyl groups for both donor and acceptor complexes, and the threonine has the same topology with its γ-methyl and hydroxyl groups. The significance of this side chain is further validated by the tunneling simulation with $_3$Val^{232} replaced with a glycine, which gives a drastic decrease of the tunneling rate (Table 1). The calculated tunneling pathway of the mutant (Fig. 2*J*) is completely different from the wild type. Because there is no residue providing a direct path, the electron makes a detour along $_3$Cys^{230} and the glycine backbone with a much longer 4.1-Å through-space jump. $_3$Pro^{231} between $_3$Cys^{230} and $_3$Val^{232} is found totally conserved, and its conformational rigidity should be critical to maintain the optimal position and orientation of the $_3$Val^{232} side chain.

The question of whether specific paths or residues were selected for electron transfer in proteins is still vigorously debated in the literature (34, 37, 38). Calculations on frozen structures clearly predict localization of the tunneling fluxes to specific structural elements of the protein. The dynamic fluctuations are expected to introduce fuzziness to this picture (36, 39); however, the inhomogeneous nature of the protein matrix still remains. Overall, there is no doubt that the tunneling barriers in proteins are not homogeneous and electrons do tunnel along specific routes in proteins. This inhomogeneity is reflected in deviations of specific rates from a universal exponential law (see Fig. S3), indicating that nether a direct through-space distance between redox sites nor a distance along a specific path —because several interfering paths may contribute—is a perfect measure of the distance dependence. Because different side chains have similar electronic structure, the mutations along the path do not dramatically change the tunneling rates, unless they introduce unfavorable empty gaps in the structure along the paths. These gaps, however, can be occupied by internal water, which as we have seen can "repair" the tunneling paths. Yet there is conservation of specific residues along the paths described above, and whether it was evolutionarily determined or not

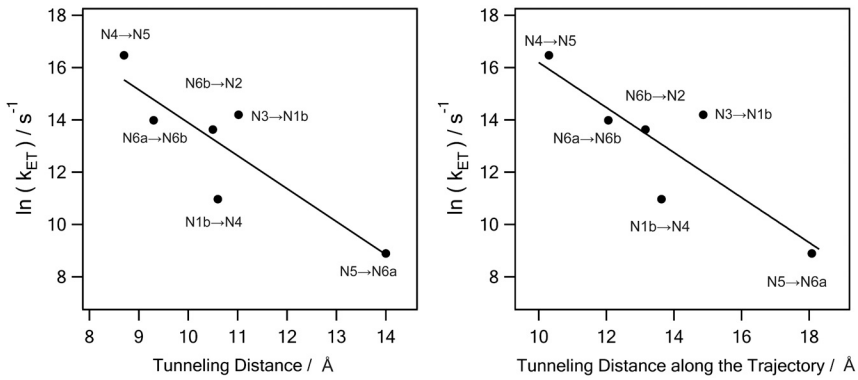

Fig. 4. Natural logarithms of the simulated electron transfer rates (in s^{-1}) versus the tunneling distance between gateway atoms (in angstroms). The negative slope of the least-squares line (solid line) is 1.3. The number is equivalent to 0.56 in base 10 logarithm, reproducing a typical value of 0.6 in proteins (37). On the right, the tunneling distance is measured along the main path; the negative slope is 0.85. The relatively slow rate for N1b → N4 transfer is because of a 1.9-Å gap along the path shown in Fig. 2*C*; the gap may be repaired by an internal water molecule in the protein.

remains to be examined further. The dynamical aspects including "gating" should also be addressed in future studies.

Conclusion

The described simulations have revealed the atomistic details of electron transfer along the whole electron transport chain from FMN to N2 in respiratory complex I; we have identified the key residues for electron transfer and demonstrated the essential role played by internal water at the interface between protein subunits as a mediator of electron transfer. The internal water has been shown to accelerate the electron transfer kinetics so as to achieve the physiologically meaningful rate. It is remarkable that the most fundamental energy-generating machinery in cells is based on the wave properties of electrons, which allow for an efficient transport of energy-carrying particles along the chain of redox cofactors toward molecular oxygen via quantum tunneling as demonstrated by this study. Together with the enzyme structure, this study provides a basis for further detailed characterization of the respiratory complex I.

Materials and Methods

The details of electron tunneling calculations, the spin state diagram of the 4Fe-4S cluster, pruning procedure, BS-ZINDO calculations, dynamical averaging of the tunneling matrix elements, and multiple sequence alignment are described in *SI Text*.

ACKNOWLEDGMENTS. This work is supported by National Science Foundation Grant PHY 0646273 and National Institutes of Health Grant GM54052.

1. Hirst J (2010) Towards the molecular mechanism of respiratory complex I. *Biochem J* 425:327–339.
2. Zickermann V, et al. (2009) Architecture of complex I and its implications for electron transfer and proton pumping. *Biochim Biophys Acta, Bioenerg* 1787:574–583.
3. Sazanov L (2007) Respiratory complex I: Mechanistic and structural insights provided by the crystal structure of the hydrophilic domain. *Biochemistry* 46:2275–2288.
4. Sazanov LA, Hinchliffe P (2006) Structure of the hydrophilic domain of respiratory complex I from Thermus thermophilus. *Science* 311:1430–1436.
5. Saraste M (1999) Oxidative phosphorylation at the fin de siecle. *Science* 283:1488–1493.
6. Lin MT, Beal MF (2006) Mitochondrial dysfunction and oxidative stress in neurodegenerative diseases. *Nature* 443:787–795.
7. Efremov RG, Baradaran B, Sazanov LA (2010) The architecture of respiratory complex I. *Nature* 465:441–447.
8. Wittekindt C, Schwarz M, Friedrich T, Koslowski T (2009) Aromatic amino acids as stepping stones in charge transfer in respiratory complex I: An unusual mechanism deduced from atomistic theory and bioinformatics. *J Am Chem Soc* 131:8134–8140.
9. Stolpe S, Friedrich T (2004) The Escherichia coli NADH:ubiquinone oxidoreductase (complex I) is a primary proton pump but may be capable of secondary sodium antiport. *J Biol Chem* 279:18377–18383.
10. Sharpley MS, Shannon RJ, Draghi F, Hirst J (2006) Interactions between phospholipids and NADH:ubiquinone oxidoreductase (complex I) from bovine mitochondria. *Biochemistry* 45:241–248.
11. Verkhovskaya ML, Belevich N, Euro L, Wikstrom M, Verkhovsky MI (2008) Real-time electron transfer in respiratory complex I. *Proc Natl Acad Sci USA* 105:3763–3767.
12. Lin JP, Balabin IA, Beratan DN (2005) The nature of aqueous tunneling pathways between electron-transfer proteins. *Science* 310:1311–1313.
13. Osyczka A, Moser CC, Daldal F, Dutton PL (2004) Reversible redox energy coupling in electron transfer chains. *Nature* 427:607–612.
14. Miyashita O, Okamura MY, Onuchic JN (2005) Interprotein electron transfer from cytochrome c(2) to photosynthetic reaction center: Tunneling across an aqueous interface. *Proc Natl Acad Sci USA* 102:3558–3563.
15. Tezcan FA, Crane BR, Winkler JR, Gray HB (2001) Electron tunneling in protein crystals. *Proc Natl Acad Sci USA* 98:5002–5006.
16. Blondin G, Girerd JJ (1990) Interplay of electron exchange and electron-transfer in metal polynuclear complexes in proteins or chemical-models. *Chem Rev (Washington, DC, US)* 90:1359–1376.
17. Noodleman L, Peng CY, Case DA, Mouesca JM (1995) Orbital interactions, electron delocalization and spin coupling in iron-sulfur clusters. *Coord Chem Rev* 144:199–244.
18. Mouesca JM, Lamotte B (1998) Iron-sulfur clusters and their electronic and magnetic properties. *Coord Chem Rev* 178:1573–1614.
19. Noodleman L, Han WG (2006) Structure, redox, pK(a), spin. A golden tetrad for understanding metalloenzyme energetics and reaction pathways. *JBIC, J Biol Inorg Chem* 11:674–694.
20. Marcus RA, Sutin N (1985) Electron transfers in chemistry and biology. *Biochim Biophys Acta* 811:265–322.
21. Gorelsky SI, Lever ABP (2001) Electronic structure and spectra of ruthenium diimine complexes by density functional theory and INDO/S. Comparison of the two methods. *J Organomet Chem* 635:187–196.
22. Lalia-Kantouri M, Papadopoulos CD, Quiros M, Hatzidimitriou AG (2007) Synthesis and characterization of new Co(III) mixed-ligand complexes, containing 2-hydroxyaryloximes and alpha-diimines. Crystal and molecular structure of [Co(saox)(bipy)(2)]Br. *Polyhedron* 26:1292–1302.
23. Ball DM, Buda C, Gillespie AM, White DP, Cundari TR (2002) Can semiempirical quantum mechanics be used to predict the spin state of transition metal complexes? An application of de novo prediction. *Inorg Chem* 41:152–156.
24. O'Brien TA, Davidson ER (2003) Semiempirical local spin: Theory and implementation of the ZILSH method for predicting Heisenberg exchange constants of polynuclear transition metal complexes. *Int J Quantum Chem* 92:294–325.
25. Karacan MS (2007) Semiempirical studies of the electronic structure of iron-sulfur proteins model compounds. *Can J Anal Sci Spectrosc* 52:25–31.
26. Newton MD (2003) Electronic coupling in electron transfer and the influence of nuclear modes: Theoretical and computational probes. *Theor Chem Acc* 110:307–321.
27. Zheng XH, Stuchebrukhov AA (2003) Electron tunneling in proteins: Implementation of ZINDO model for tunneling currents calculations. *J Phys Chem B* 107:6621–6628.
28. Torres RA, Lovell T, Noodleman L, Case DA (2003) Density functional- and reduction potential calculations of Fe4S4 clusters. *J Am Chem Soc* 125:1923–1936.
29. Stuchebrukhov AA (2001) Toward ab initio theory of long-distance electron tunneling in proteins: Tunneling currents approach. *Adv Chem Phys* 118:1–44.
30. Stuchebrukhov AA (2003) Long-distance electron tunneling in proteins. *Theor Chem Acc* 110:291–306.
31. Stuchebrukhov AA (2003) Tunneling currents in long-distance electron transfer reactions. V. Effective one electron approximation. *J Chem Phys* 118:7898–7906.
32. Gehlen JN, Daizadeh I, Stuchebrukhov AA, Marcus RA (1996) Tunneling matrix element in Ru-modified blue copper proteins: Pruning the protein in search of electron transfer pathways. *Inorg Chim Acta* 243:271–282.
33. Page CC, Moser CC, Chen XX, Dutton PL (1999) Natural engineering principles of electron tunnelling in biological oxidation-reduction. *Nature* 402:47–52.
34. Gray HB, Winkler JR (2007) Electron transfer through proteins. *Biological Inorganic Chemistry, Structure and Reactivity,* eds I Bertini, HB Gray, EI Stiefel, and JS Valentine (University Science Books, Mill Valley, CA), pp 261–277.
35. Dutton PL, Moser CC, Sled VD, Daldal F, Ohnishi T (1998) A reductant-induced oxidation mechanism for complex I. *Biochim Biophys Acta, Bioenerg* 1364:245–257.
36. Daizadeh I, Medvedev ES, Stuchebrukhov AA (1997) Effect of protein dynamics on biological electron transfer. *Proc Natl Acad Sci USA* 94:3703–3708.
37. Moser CC, Page CC, Dutton PL (2006) Darwin at the molecular scale: Selection and variance in electron tunnelling proteins including cytochrome c oxidase. *Philos Trans R Soc Lond, Ser B* 361:1295–1305.
38. Beratan DN, Balabin IA (2008) Heme–copper oxidases use tunneling pathways. *Proc Natl Acad Sci USA* 105:403–404.
39. Balabin IA, Onuchic JN (2000) Dynamically controlled protein tunneling paths in photosynthetic reaction centers. *Science* 290:114–117.